Flow Instabilities, Energy Levels, and Structure in Stirred Tanks

Jesper Kilander, Fredrik J. E. Svensson, and Anders Rasmuson
Chemical Engineering Design, Dept. of Chemical and Biological Engineering, Chalmers Univ. of Technology, S-412 96 Göteborg, Sweden

DOI 10.1002/aic.11036
Published online October 30, 2006 in Wiley InterScience (www.interscience.wiley.com).

In this study, the spatial distribution and significance of macro instabilities in two cylindrical tanks of different size, and one square tank, stirred with standard six bladed Rushton impellers, are investigated. The instabilities of the flow structure are investigated by searching for significant frequencies using the Lomb algorithm on instantaneous velocity data collected using laser Doppler anemometry at various locations in the tanks. The investigation of the energy levels shows that the harmonics of the blade passage differ in both magnitude and spatial distribution for different tank sizes, geometries, and energy input. Several significant dimensionless frequencies, that is, frequency Strouhal numbers, are detected and identified both in relative magnitude and spatial range. © 2006 American Institute of Chemical Engineers *AIChE J,* 52: 4039–4051, 2006
Keywords: mixing, macro instabilities, frequency analysis, stirred tank, Rushton turbine

Introduction

Tank reactors that are stirred by one or more impellers are widely used in the chemical process industry. Agitation is important since it promotes mixing/blending, heat transfer, and mass transfer. Numerous studies regarding stirred tanks have been performed in the past, and it is generally accepted that the mean flow in stirred tanks with standard configuration is fairly well understood.[1] However, the instantaneous flow induced by an impeller becomes extremely complex as it interacts with vessel geometry, for example, baffles, walls, and other impellers within the tank. Fluctuations in the mean flow range from high frequency turbulence that controls and limits, for example, micro-mixing, agglomeration, and break-up phenomena, to quasi-stationary low frequency phenomena that affect flow patterns, and consequently the mixing performance. These phenomena are commonly referred to as macro-instabilities (MI).

Early work regarding vessels stirred with axial pumping impellers have identified MI as a consequence of double loop flow patterns,[2,3] and a linear relationship between impeller speed (N) and the frequency of the MI (f_{MI}) have been found. Chapple and Kresta[4] have concluded that the MI occur due to geometry, for example, walls and baffles, and that these are linked to turbulence intensity. The investigation by Bakker and Van den Akker[5] using computational fluid dynamics (CFD) shows that interaction between two opposite vortex motions induces large scale instabilities in the flow in a tank stirred with an axial pumping pitch blade turbine (PBT). Also using a PBT, Montes et al.[6] have found MI that appear as the switching between loops in the large scale three-dimensional vortex structure. These were found in the top of the tank and around the baffles and appeared on a regular basis. The instabilities were more regular for lower Reynolds numbers.

Kresta[7] has reported that two separate MI phenomena exist. One corresponds to blade passage frequencies (BPF), and the other corresponds to large scale structures of the flow. Hasal et al.[1] have used a proper orthogonal decomposition technique and image analysis to investigate the MI with spatial resolution in a PBT stirred vessel. They have determined that the length scales of MI are comparable to the size of the vessel. The MI in the study are more pronounced in the transitional flow regime and are hardly detectable at high Reynolds numbers. However, Roussinova and Kresta[8] have found, using a

Correspondence concerning this article should be addressed to A. Rasmuson at rasmuson@chemeng.chalmers.se.

PBT, that the frequency Strouhal number, $St = f_{MI}/N$, is constant for Re $> 10^4$. The value of St defined in this way is different from the classical Strouhal number by the factor d/D.[9] They have also concluded that no dominating frequency is found for the A310 and HE3 impeller regardless of off-bottom clearance. Later studies by Roussinova et al.[9] show that f_{MI} scales linearly with the rotational speed for Re $> 2{\cdot}10^4$. In the same study, it is shown that large eddy simulations (LES) are able to predict the Strouhal number ($St = 0.186$) for the same configuration. Using the LES simulations, they have identified three mechanisms for the induction of MI: the pressure fluctuations due to reflections of impinging jets, converging radial flow at the bottom of the tank, and shedding of trailing vortices from the impeller blades.

Roussinova et al.[10] have continued to study the same system and have determined that the propagation and coherence of the previously identified MI are dependent on specific conditions, such as impeller design and tank geometry. Galletti et al.[11] have used laser Doppler anemometry (LDA) to study the effect of off-bottom clearance in a vessel stirred with a Rushton turbine. They have found three types of flow: the double loop regime, the transitional regime, and the single loop regime. The transitional regime is characterized by periodic fluctuations of all three flow patterns in the order of minutes, indicating the importance of sufficient data collection time to ensure that the lifetime of the fluctuation is exceeded. They have found a linear dependence between the characteristic frequency and the rotational speed in the unstable transitional type flow pattern between the double and single loop pattern, resulting in a characteristic $St = 0.12$. Galletti et al.[12] have found that the previously discussed linear dependence between the frequency of the MI and the rotational speed of the stirrer exhibits different proportionality constants for low, intermediate, and high Reynolds number flows. They have also found, using both a PBT and a Rushton turbine, that the off bottom clearance of the impeller has no significant effect on the frequency of the MI. They did, however, find that the frequency changed when the ratio between the impeller diameter and the tank diameter changed.

Nikiforaki et al.[13] have also studied the influence of impeller clearance and design. They have reported that a fundamental frequency with a frequency Strouhal number between 0.015–0.02 is present for both the Rushton turbine and the PBT in all configurations. However, the relative importance of the harmonic BPF is dependent on configuration tank and geometry. They have identified a precessional motion about the impeller axis as the source of the MI. The same whirlpool type vortex was pointed out by Yianneskis et al.[14] Hartmann et al.[15] used LES in order to quantify the whirlpool type precessing vortex in terms of characteristic frequency and fluctuation levels. They have found $St = 0.0255$ and $St = 0.0228$ for $Re = 2{\cdot}10^4$ and $Re = 3{\cdot}10^4$, respectively. They have also found a laminar frequency with $St = 0.092$ for $Re = 10^4$. These MI differ in time scale from the circulation type MI resolved through LES simulations by Russinova et al.[9] Further, Nikiforaki et al.[13] report that turbulence levels are broadened up to 25% by superimposed macro instability flow patterns. Later studies by Nikiforaki et al.[16] show that RMS levels are increased by 23% by the presence of MI.

Macro instabilities complicate flow patterns and constitute a force that can damage mechanical parts in the system and influence mixing performance.[1] It is, therefore, important to have a clear understanding of resonance geometries and frequency Strouhal numbers when designing mixing equipment for the process industry. Also, a recent study has found a linear relationship between the intermittency phenomena,[17] that is, temporal and spatial variability of local values of energy dissipation, and the MI in the bulk flow. It is, therefore, of interest to gain an understanding of the spatial distribution of the macro instability phenomena since intermittency is important when modeling, for example, drop/floc breakage,[18] because of its relation to turbulent mechanical stress. Consequently, this warrants further investigation into the nature and cause of low frequency phenomena separated from the mean flow.

There appear to be two main varieties of MI: the circulation type MI that only appears under certain conditions, and the precessing type vortex MI that are found in most configurations. It is interesting to investigate the interactions between these types of MI in terms of energy levels and spatial distribution, especially for high Reynolds flow where turbulence becomes more intermittent. In the present study, periodic instabilities in the flow field are investigated by searching for significant frequencies using the Lomb algorithm[19] on velocity data collected using LDA at various distances from the impeller in two cylindrical tanks of different size, and one square tank. The spatial distribution of energy levels and macro instabilities is measured and presented in detail. The results explain some of the deviating results obtained in the past where only a few measuring points were utilized.

Frequency Analysis

The theory of the energy cascade as presented by Kolmogorov[20] describes a separation in interaction between large energy containing eddies and small dissipative scale eddies. However, energy is cascaded through the entire spectrum of turbulent kinetic energy. It is also assumed that there are no fluctuations in the local values of the rate of energy dissipation, ε. Thus, the kinetic energy spectrum can be described by Eq. 1:

$$E(\kappa) = C_k \varepsilon^{2/3} \kappa^{-5/3} \tag{1}$$

where κ is the wave number and C is the universal Kolmogorov constant. The one-dimensional energy spectrum derived from the spatial Fourier mode and the two-point auto-correlation function can in homogeneous isotropic turbulence be written as:[21]

$$k = \frac{1}{2}\langle u_i u_i \rangle = \int_0^\infty E(\kappa, t) d\kappa \tag{2}$$

where k is the kinetic energy and $\langle u_i u_i \rangle$ is the trace of the velocity tensor. The energy spectrum in this study is calculated using the Lomb algorithm.[17,22,23]

Experimental

Apparatus

Three different tanks were used in this study, two cylindrical, with identical geometry, albeit baffle width and scale dif-

Table 1. Tank Configurations

Parameter	Notation	Small Tank	Large Tank	Square Tank
Tank diameter (inner)	T	0.14 m	0.29 m	0.31 m
Number of baffles	n_b	4	4	none
Baffle width	w_b	T/12	T/10	–
Liquid height	H	T	T	T

fered, and one square tank. The geometries of the tanks are shown in Table 1.

The bottoms of the tanks were flat, and there were no lids on top of the liquid. The cylindrical vessels were made of Perspex glass, and the square tank was made of standard glass. The baffles and impellers were painted black in order to minimize reflections that might interfere with the receiving optics. The impellers used in the experiments were standard six bladed Rushton impellers with no hub. The impeller disc was welded directly onto the shaft. Details of the impeller geometry are given in Table 2.

The cylindrical tanks were placed inside a square tank in order to minimize optical distortions while measuring off-axis and to make the positioning of the measuring volume created by the intersecting laser beams easier.

Magnitude of stirring and energy input

The impeller speed was kept constant at two levels of energy input per unit volume. The basis for the revolution rate was Reynolds numbers of 18,600 and 49,100, respectively, for the small cylindrical tank and the square tank. At higher levels there was air entrainment. Keeping the impeller power number constant[24] allowed for the following expression to be used in order to obtain the revolution rates for the other levels:

$$N_2 = N_1 \cdot \left(\frac{V_2}{V_1}\right)^{1/3} \cdot \left(\frac{D_1}{D_2}\right)^{5/3} \tag{3}$$

The revolution rates were equal to a tip speed of 1.06 m/s and 1.26 m/s in the small tank, 1.36 m/s and 1.57 m/s in the large cylindrical tank, and 1.55 m/s in the square tank.

Laser Doppler anemometry equipment

The LDA system used in this study was commercially obtained from Dantec Measurement Technology. The system consisted of a FiberFlow dual beam system (Series 60X) and a Spectra-Physics water cooled 7W Ar-ion laser, model 2060A-64. The only channel used was 514.5 nm, which had an output effect of 1.9W. A frequency shift of 40 MHz was applied, giving a maximum measurable velocity of around 90 m/s. A Dantec 60X83 lens giving a focal length of 310 mm and an expansion factor of 1.98 was used. The probe included the receiving module and was thus operated in backscattering mode. The probe was mounted on a traversing system allowing the probe to be traversed 1 m in the horizontal direction and 0.8 m in the vertical direction with an accuracy of 12.5 μm (80 pulses per mm). The beams of 514.5 nm with a separation of 67.5 mm after expansion formed a measuring volume with a length of 0.702 mm, a height of 0.076 mm, and a width of 0.076 mm. The distance between two fringes was approximately 2.378 μm, and the measurement volume consisted of 32 fringes. The number of samples in each burst was set to 64, and the equipment was operated in the burst signal mode. Location information, velocity, and arrival and transition time were then stored and post-processed in the Windows based BSA Flow Software, version 2.12.00.15, program. The operating parameters of the laser and the receiving and amplifying equipments were tuned at each set of measuring points in order to obtain the highest possible data rate validation. The signal gain was varied from 23 to 32 dB, and the high voltage was changed from 1300 to 1650V. After a test was initialized, the only operating parameter that was changed during the experimental run was the effect of the laser, which was adjusted manually during the experiments.

Measurement conditions and locations

Deionized tap water, at room temperature, was used as the working fluid in all experiments in this study. Silver-coated hollow glass spheres supplied by Dantec were used as tracer particles. The diameter of the particles was 10 μm, and the density was 1,300 kg/m^3.

The overall flow structure induced by the impeller was measured in two planes. These two planes were chosen in order to investigate the importance and spatial distribution of impeller induced periodic fluctuations, and to study the relative magnitude and distribution of low frequency MI.

In the first plane, the axial and radial velocities were measured from the baffle to the impeller tip in all three tanks. This plane was situated straight towards the baffle in the cylindrical case and towards the midpoints of the wall in the square case. The plane was centered vertically according to IC +/− 1.5W (IC = Impeller Center). In the small and large cylindrical tanks, the distance between the measurement positions was 2 and 3 mm, respectively, in the horizontal and vertical directions. In the square tank, the distance between measuring points was 4 mm in both directions.

Tangential and axial velocities were measured in a second plane located from the top to the bottom of the cylindrical tanks, midway between the baffles. The distance between measuring points in the small cylindrical tank was 3 mm in both the vertical and horizontal directions. In the larger cylindrical tank, the distances were 5 mm and 10 mm in the vertical and horizontal directions, respectively.

The impeller region in the small cylindrical tank is denoted I, III in the large cylindrical tank, and V in the

Table 2. Impeller Configuration

Parameter	Notation	Value
Impeller diameter	D	T/3
Impeller clearance	C	T/3
Impeller submergence	S	2T/3
Number of blades	n_{bl}	6
Blade angle	β	90°
Blade width	W	D/5
Blade length	B	D/4
Blade thickness	x_{bl}	D/50
Disc thickness	x_d	D/50
Disc diameter	D_d	6D/10

Table 3. Summarized Measurement Conditions

Notation	Tank	Velocity Component	Revolution Rate [min^{-1}]	Tip Speed [ms^{-1}]	Reynolds Number	Number of Points
I a	small cylindrical	axial	448	1.08	16,100	17 * 16
I b	small cylindrical	radial	448	1.08	16,100	17 * 16
I c	small cylindrical	axial	517	1.26	18,600	17 * 16
I d	small cylindrical	radial	517	1.26	18,600	17 * 16
II a	small cylindrical	axial	448	1.08	16,100	5 * 42
II b	small cylindrical	tangential	448	1.08	16,100	5 * 43
II c	small cylindrical	axial	517	1.26	18,600	5 * 42
II d	small cylindrical	tangential	517	1.26	18,600	5 * 43
III a	large cylindrical	axial	260	1.36	43,000	22 * 21
III b	large cylindrical	radial	260	1.36	43,000	22 * 21
III c	large cylindrical	axial	300	1.57	49,700	22 * 21
III d	large cylindrical	radial	300	1.57	49,700	22 * 21
IV a	large cylindrical	axial	260	1.36	43,000	5 * 53
IV b	large cylindrical	tangential	260	1.36	43,000	5 * 55
IV c	large cylindrical	axial	300	1.57	49,700	5 * 53
IV d	large cylindrical	tangential	300	1.57	49,700	5 * 55
V a	square	axial	296	1.55	49,100	24 * 16
V b	square	radial	296	1.55	49,100	24 * 16

square tank. The second plane midway between the baffles is denoted II in the small cylindrical tank and IV in the large cylindrical tank. For reasons of brevity, only three lines from each measurement case will be presented and discussed. The experimental measurement configurations are summarized in Table 3, and the locations are indicated in Figures 1 (small cylindrical tank) and 2 (square tank). Lines denoted A, B, and C were located at distance from the bottom IC + 1.5W, IC, and IC − 1.5W, respectively. Lines D, E, and F were located midway between the baffles, with line D being closest to the impeller and F closest to the tank wall. Line D was located 18 and 57 mm from the wall in the small and large tank, respectively. The location of line E was midway between line D and F. The distance between the wall and line F was 3 mm in the small tank and 7 mm in the large tank.

The LDA system operated in burst mode, and around 10^5 validated samples were collected at each measuring point. The average acquisition rate varied from 250 Hz at the top part of the tank to 2000 Hz at the impeller jet, thus yielding acquisition times of 400 s to 50 s, respectively. This means that the turbulence scales could be resolved and that low frequency phenomena could be captured with a sufficient number of periods within the acquisition time.[10]

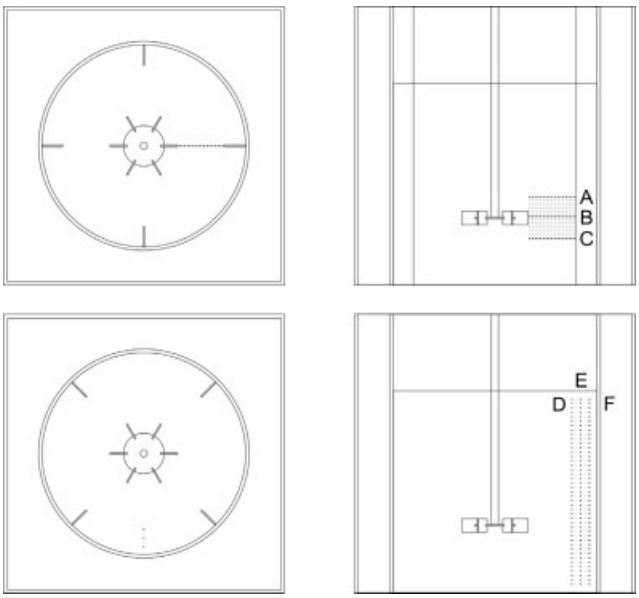

Figure 1. Measurement locations in the small cylindrical tank from above (left) and from the sides (right).

The top images indicate location I for axial and radial measurements; and the lower images indicate position II, tangential, and axial measurement positions.

Results and Discussion

The bottom-flow-loop in the characteristic double loop flow structure that is induced by radial impellers such as the Rushton turbine has a mean circulation time that is far less than the top-flow-loop. The interactions between these two loops are often referred to as an induction phenomenon for MI.[11] Also, the interactions between the impeller stream and the trailing vortices produce periodic fluctuations that require

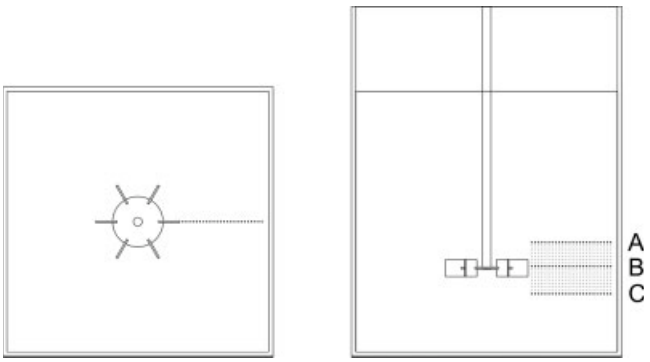

Figure 2. Measurement locations in square tank from above (left) and from the sides (right).

The images indicate location V for axial and radial measurements positions.

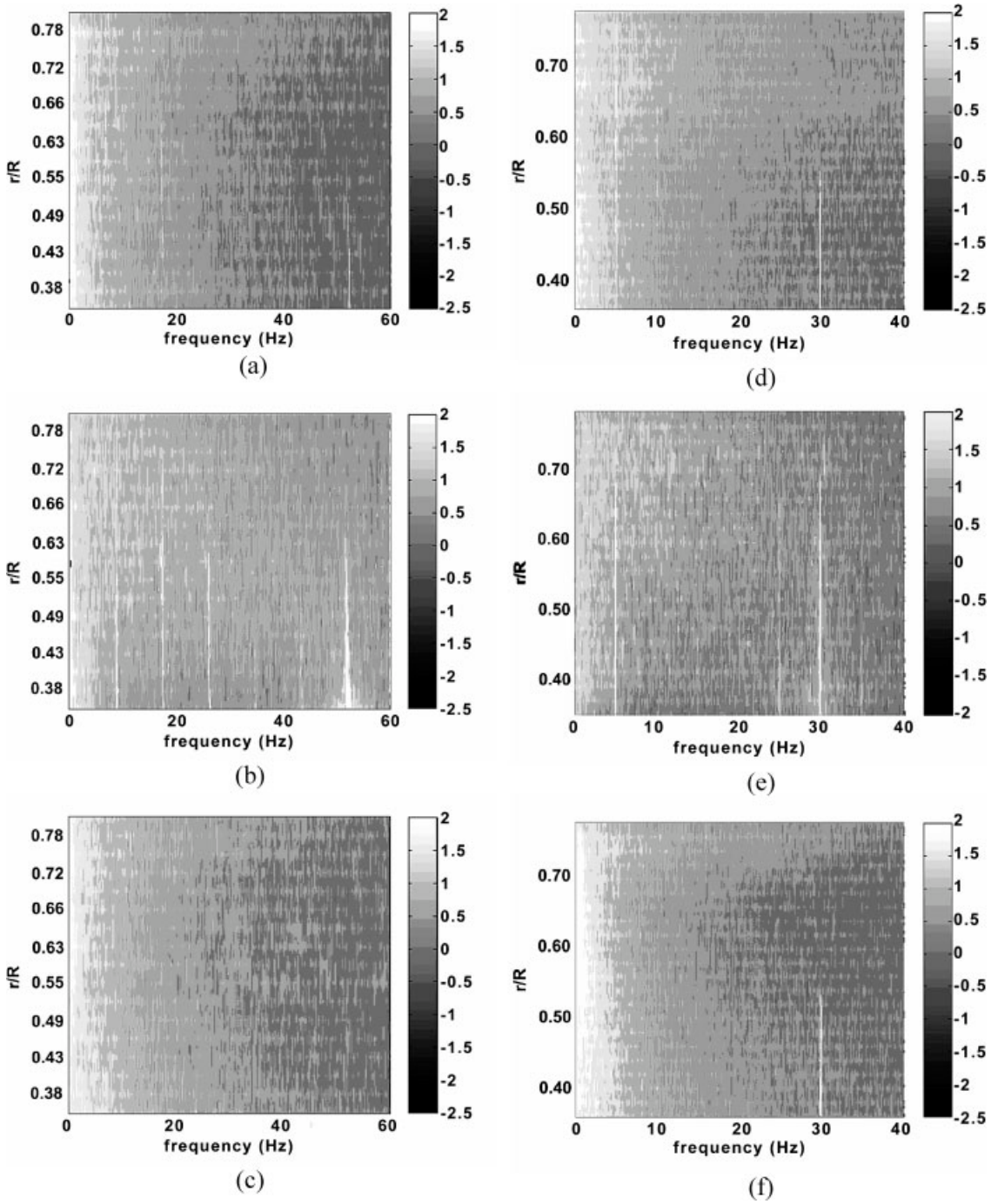

Figure 3. The spatial distribution of energy levels in the impeller stream.

Graphs (a), (b), and (c) denote measurement configuration Id; and graphs (d), (e), and (f) denote IIId. The top graphs show measuring line A, the middle graphs show measuring line B, and the bottom graphs show measuring line C.

phase averaging, that is, correlation of the impeller blade position in time with the measurements, if true turbulent fluctuations are to be measured directly. The velocity fluctuations associated with the blade passage are often treated as pseudo turbulence since they are not completely random.[25] This pseudo turbulence will increase the RMS values in a non-random fashion. It is often argued that it is necessary to remove the pseudo turbulence in order to properly characterize the turbulence.[26] However, Kresta and Wood[2] argue that the trailing vortices are similar to random large scale eddies found in other types of shear flow. They have found that removal of the pseudo turbulence has no impact on mean and fluctuating velocities and that periodically generated vortices can be treated in the same way as randomly occurring vortices—although studies performed by Pettersson and Rasmuson[27] show that the RMS can be overestimated by as much as 30% when not using phase averaging on the collection of the velocity data. In this study, however, the objective was to

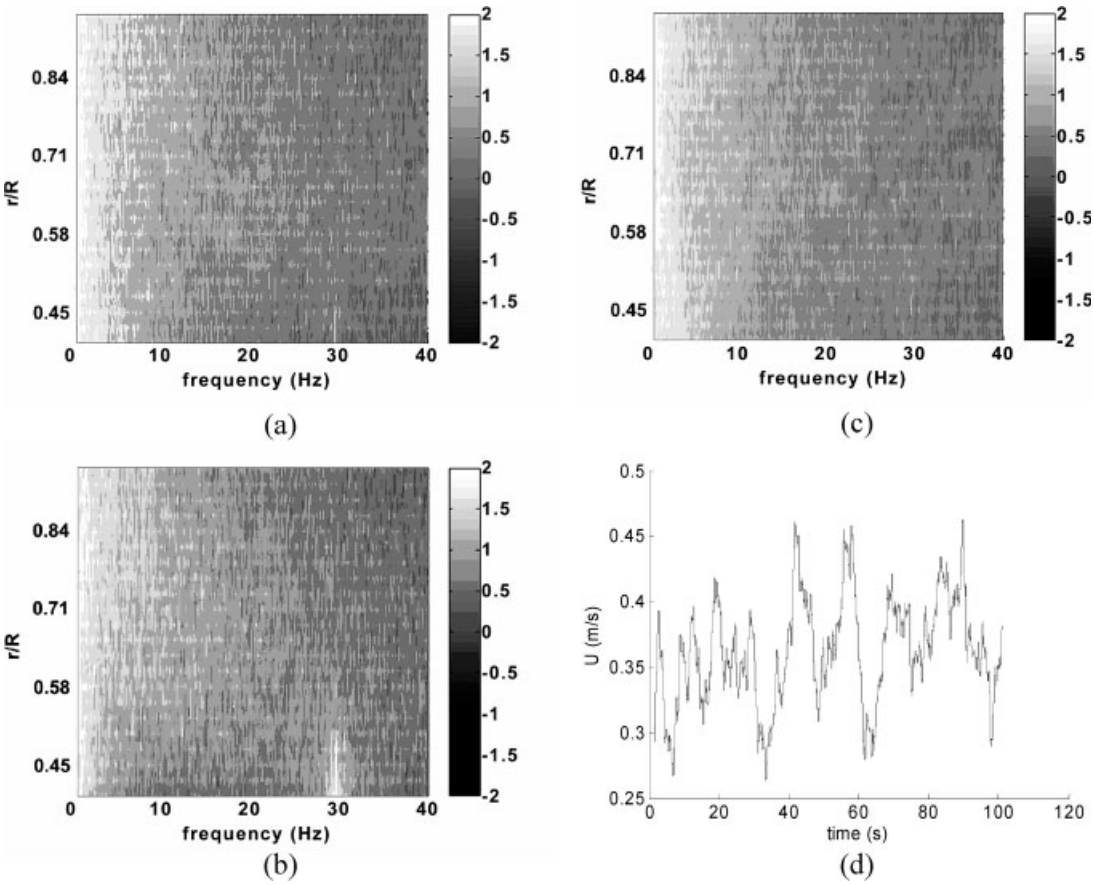

Figure 4. The spatial distribution of energy levels in the impeller stream for measurement configuration Vb.

Graph (a) shows measuring line A, graph (b) shows measuring line B, and graph (c) shows measuring line C. Graph (d) shows the time evolution of the velocity at height = C and r/R = 0.76 using a moving average of 1331 samples.

follow all instabilities in the flow; thus, no phase averaging was performed.

Spatial distribution of significant energy levels

The Impeller Stream in Cylindrical Tanks. The distributions of energy levels in the impeller stream are shown in this section. The graphs show the spatial distribution of the significant frequencies along a line of interest; see Figures 1 and 2. For example, if Figure 3f is studied, it reveals that only the 5th harmonics of the BPF (30 Hz) is detected in the bottom of the impeller stream, along line C, Figure 1. Also, it can be established that the disturbance fades at a point (r/R = 0.53) towards the wall of the vessel. It can also be seen that there is a minimum in energy in the area 20 to 40 Hz and $0.5 < r/R < 0.7$, which suggests a local difference in flow properties. The scales in Figures 3 and 4 show the logarithm of the power spectral density (PSD). Thus, the vertical lines that are visible in Figures 3 and 4 are several orders of magnitude more significant than the background. In essence, Figures 3 and 4 give the opportunity to study local flow properties in regard to instabilities induced by the impeller.

Figure 3 shows the distribution of energy levels for the small and large cylindrical tank (configurations Id and IIId). The energy levels at frequencies 51.7 Hz and 30 Hz representing the 5th harmonics from the six bladed Rushton turbine for impeller speeds 517 rpm and 300 rpm are visible in the middle graphs. The 5 Hz BPF is visible along line A for the large cylindrical tank, Figure 3d. Generally, more energy is found in the lower frequency band as compared to higher frequencies.

The BPF and impeller blade harmonics can be seen clearly in the middle of the impeller stream, as indicated by Figures 3b and 3e denoting measuring line B. The 4th and the 5th harmonics of the BPF are visible in the large cylindrical tank, whereas more blade passage frequencies can be seen in Figure 3b depicting the small cylindrical tank. In Figure 3e, the 1st, 2nd, and 3rd harmonics are not visible, indicating a more even impeller stream flow. The inertia of low frequency fluctuations is greater in the large cylindrical tank than in the small cylindrical tank. When comparing the time evolution of the velocity, Figure 5a, between the two vessel sizes in the low energy cases, it is obvious that the variations are greater and the fluctuations are more erratic in the smaller tank. There is a large difference in Reynolds number between the two configurations, 16,100 and 43,000, respectively, for the small and the large tanks. It has previously been reported that MI are found predominantly in low to intermediate flows.[12]

There is also a 6th harmonics visible in Figure 3e for the large cylindrical tank case, a "ghost frequency" since the impeller only has 6 blades. A plausible explanation can be that wobbling of the impeller axis acts as a 7th blade, frequency wise.

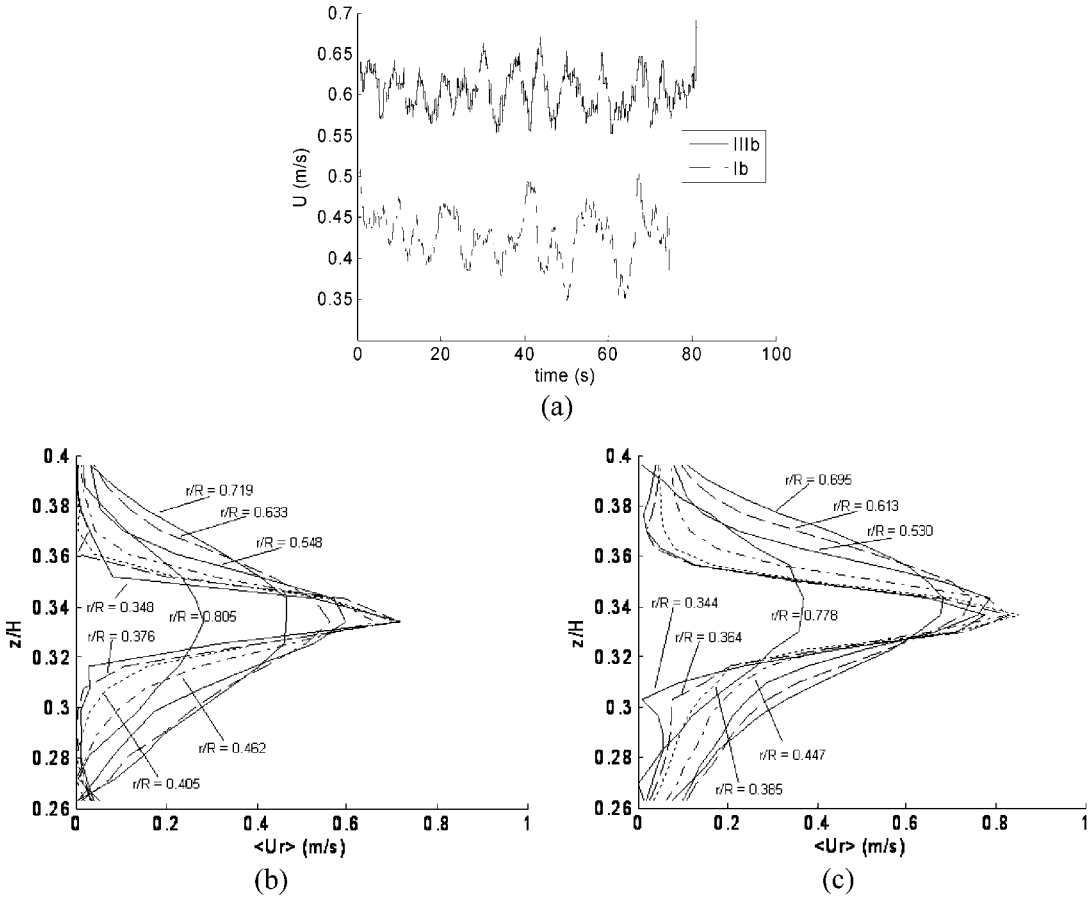

Figure 5. Top graph: The time evolution of the velocity at height = C and r/R = 0.76 for cases Ib and IIIb using a moving average of 2,331 samples.

Bottom graphs: Velocity profile over the impeller stream with parameter r/R. (b) Case Id and (c) Case IIId.

The velocity profiles for the radial component over the impeller stream are also different in shape, as can be seen in Figures 5b and 5c, representing intermediate and high Reynolds number, respectively. The stream profile is more asymmetric in the case of the large cylindrical tank in compliance with the results of Wu and Patterson,[26] but the velocity profile in both cases broadens by several blade widths as it approaches the baffle. The top of the impeller stream in the large tank is broadened more than the bottom part. Also, the location of the highest radial velocity for the large tank case is not constant with regard to z/H. The stream is pointing upwards as it approaches the baffle. This also compares well with the result of Wu and Patterson,[26] who looked at a tank size comparable to the current but with a revolution rate of 200 rpm. This phenomenon is not as pronounced in the small tank case.

The Impeller Stream in Square Tanks. The square tank demonstrates a very different scenario. In Figure 4b representing line B, it can be seen that the significance of the 5th harmonics of the impeller frequency at 29.6 Hz fades very quickly away from the impeller.

The same phenomenon is reported in the investigation of the flow field in a square tank by Kilander and Rasmuson,[23] using the axial flow Lightnin A310 hydro foil impeller. It seems that the effect of the impeller is very local in the square configuration, regardless of impeller type. The fluctuations are very large and regular, as shown in the graph of the time evolution of the radial velocity. This indicates a stable circulation type MI for the square configuration. The relative size and exact frequency of these MI is examined below. The distribution of low frequency structures is similar at the top of the impeller stream (line A) and at the bottom of the stream (line C) for the square configuration. This was not the case in the cylindrical vessels.

Influence of the Walls in Cylindrical Tanks. Figure 6 shows the distribution of the energy levels along lines D, E, and F for the small and large cylindrical tanks when measuring the axial velocity component for the higher energy input case (measuring configurations IIc and IVc). The influence of the impeller stream decreases when the distance to the wall decreases; however, Figures 6a, 6b, 6d, and 6e representing lines D and E show that the impeller stream influences the entire studied frequency band. This phenomenon is more pronounced for the large tank; the area of influence is more defined, again reflecting on the greater inertia of the impeller stream in the large tank. It is also interesting to notice that the impeller stream seems to cancel out low frequency structures, that is, there is a minimum present in the area ~2.5 Hz and z/L ~ 0.35, seen most clearly in Figures

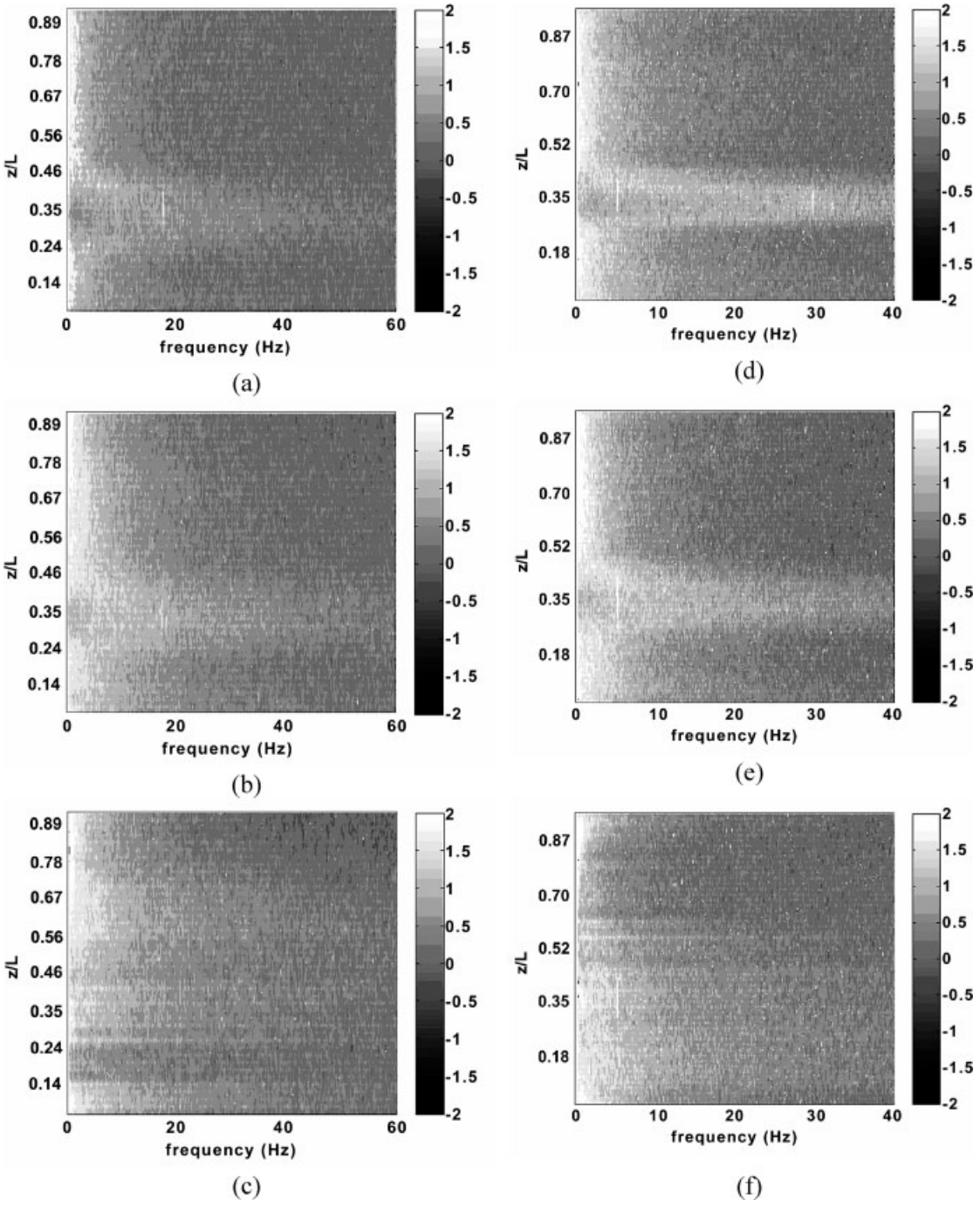

Figure 6. The spatial distribution of energy levels between the baffles.

Graphs (a), (b), and (c) denote measurement configuration IIc; and graphs (d), (e), and (f) denote IVc. The top graphs show measuring line D, the middle graphs show measuring line E, and the bottom graphs show measuring line F.

6a, 6b, 6d, and 6e. It can also be seen that the part of the tank that is influenced by the impeller stream widens as distance to the wall decreases. This is to be expected, since the impeller stream widens towards the wall. At measuring line F, graphs 6c and 6f, closest to the wall of the tank, the influence of the impeller is not readily visible; however, the 5 Hz BPF in the large tank can clearly be seen in graph 6f at z/H $\sim$ 0.35. We can, therefore, state that the walls have a damping and spreading out effect on the instabilities, most likely due to interference phenomena. It is also clear from the graphs that the influence of low frequency phenomena can be seen in the entire height of the tank.

Spatial distribution of low frequency phenomena (MI)

The Impeller Stream in Cylindrical Tanks. The study of the dimensionless frequencies present in the systems investigated in the following section is limited to the Strouhal num-

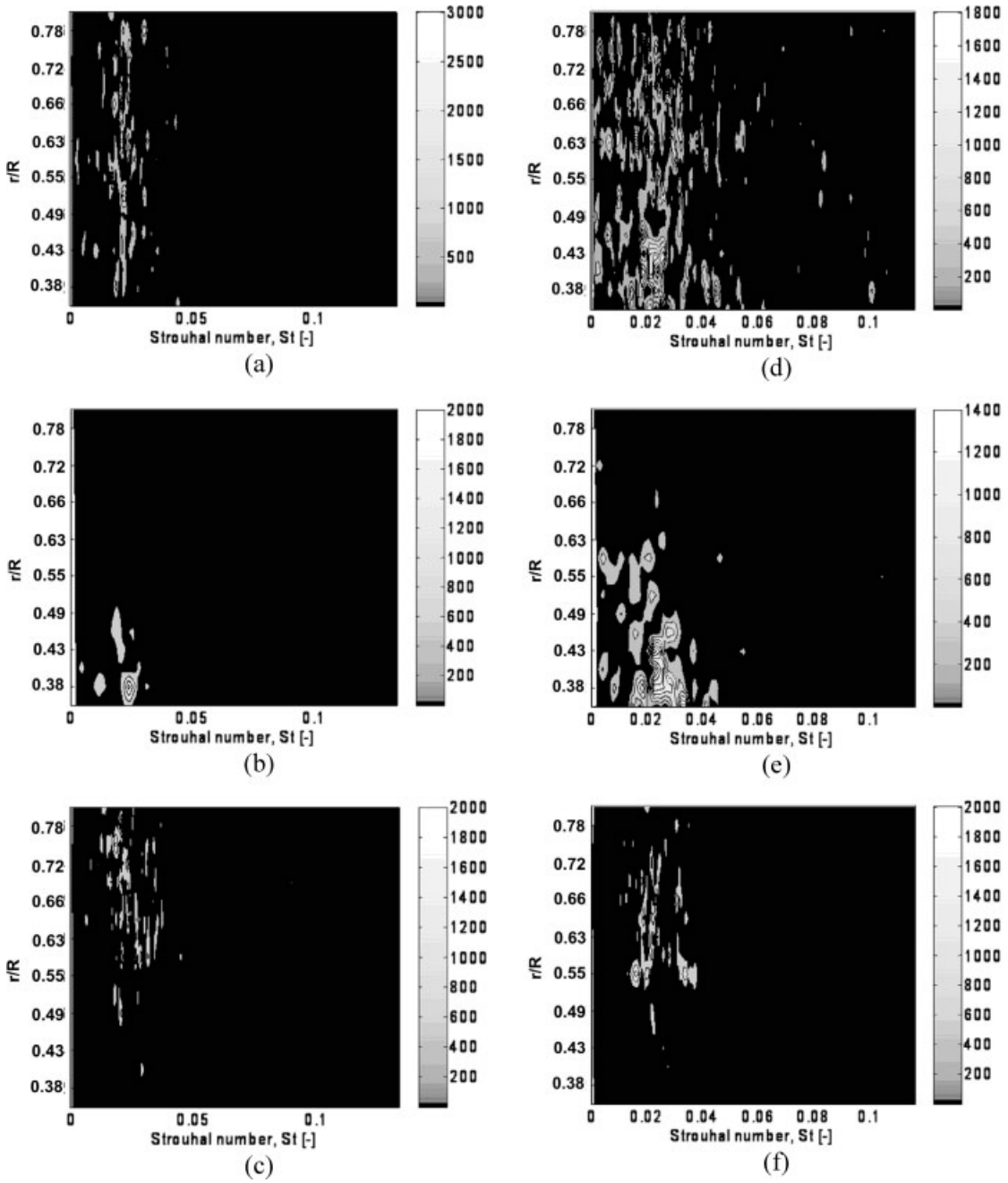

Figure 7. The spatial distribution of macro instabilities in the impeller stream.

Graphs (a), (b), and (c) denote measurement configuration Ib; and graphs (d), (e), and (f) denote Id. The top graphs show measuring line A, the middle graphs show measuring line B, and the bottom graphs show measuring line C.

bers for MI present between 0 to 1 Hz. Thus, the maximum Strouhal numbers investigated in the small vessel are 0.133 (in the 448 rpm case) and 0.116 (in the 517 rpm case), and in the large vessel 0.231 and 0.200 for the 260 and 300 rpm cases, respectively. The macro instabilities in the impeller stream for the small cylindrical tank are shown in Figure 7.

Figures 7a–7c show the 448 rpm case, and Figures 7d–7f show the 517 rpm case. It is clear from the pictures that there is a dominant frequency around St = 0.02–0.03. A closer investigation yields that the disturbance in measurement configuration Ib (448 rpm) is centered around St $\approx$ 0.025—the same dimensionless frequency found by Hartmann et al.[15] using LES in their investigation of the whirlpool type precessing vortex. Hartman et al.[15] also found that increasing the Reynolds number from $Re = 2{\cdot}10^4$ to $3{\cdot}10^4$ decreases the dimensionless frequency slightly to $St = 0.0228$.

In the present study, however, it is difficult to assess the changes in the dimensionless frequency with increasing Reynolds number since a comparison with the disturbance for measurement configuration Id (517 rpm), depicted in Figures 7d–7f, clearly shows an increase in the bandwidth. Fig-

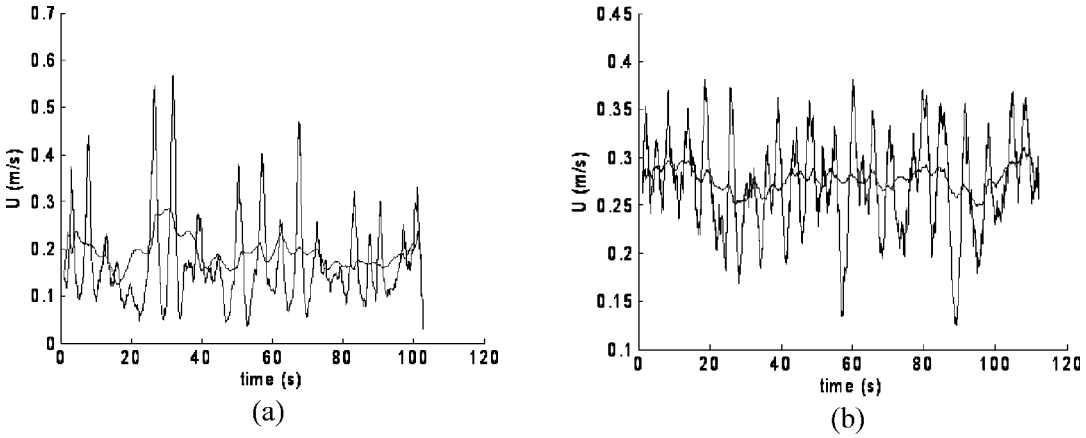

Figure 8. The time evolution of the velocity in case Id on measuring line B, for (a) at r/R = 0.46, and for (b) at r/R = 0.76.

The values were obtained by using a moving average of 1,331 and 13,331 samples, where the latter one is the more smoothed line.

ures 7a and 7d depicting measuring line A, that is, above the impeller, show that the spatial distribution of the MI ranges from the impeller to the baffle, whereas the MI in the middle of the impeller stream decreases after a third and a little more than half of the length between the impeller and the baffle in the 448 rpm and 517 rpm cases, respectively. This phenomenon is also noticed in Figures 6a and 6d representing line D and Figures 6b and 6e representing line E, where it can be seen that there exists an energy minimum in the impeller jet at low frequencies. Thus, we would expect that the time evolution of the velocity would differ depending on where in the impeller stream the measurement point is selected. Figure 8 examines the time evolution of the velocity for the small cylindrical tank (measuring configuration Id). Figure 8a shows the time evolution at a point r/R = 0.46 along measuring line B, that is, before the St $\approx$ 0.02 MI is cancelled by the jet stream. Figure 8b shows a point r/R = 0.76 along line B, that is, after the St $\approx$ 0.02 MI is cancelled by the stream.

It is clear that there is a difference in the type of flow before and after the St $\approx$ 0.02 MI is cancelled at a point between $0.46 < r/R < 0.76$. The MI canceling point between the two types of flows coincides with the end of the plateau of the maximum radial velocity in the radial velocity profile; see Figure 9. Also, Figure 8 shows a very long period of MI, depicted by the line using the 13,331 sample moving average, again stressing the importance of location when measuring macro instabilities.

The results for the MI in the impeller stream in the large cylindrical vessel show that there is a drastic increase in the level of noise, and the amplitudes of the instabilities are lower than in the small vessel. Galletti et al.[12] also found that for high Reynolds numbers, the amplitudes of the peak frequencies are smaller than those of low Reynolds numbers. However, in this study, the maximum amplitude instabilities are still found at St $\approx$ 0.02–0.03. The maximum amplitudes are as much as 15 times greater in the case of the small vessel, that is, a smaller Reynolds number.

The Impeller Stream in Square Tanks. Although there are high amplitude instabilities present in the impeller stream for the square tank configuration, there is still a lot of noise above the impeller, at measuring line A, and in the middle of the impeller stream, at measuring line B. This is to be expected, since the flow is in the high Reynolds number range. However, two distinct MI could be found in the investigation of measuring line C. The dimensionless frequencies found were St $\approx$ 0.01 and St = 0.06–0.07. The first MI, St = 0.01 corresponds to a period of 20.3 s. This time period is also visible in Figure 4 in the time evolution of the velocity.

Macro Instabilities Near the Wall in Cylindrical Tanks. The MI near the wall for the small vessel configuration (cases IIc and IId) are shown in Figure 10. The instability with St = 0.0255 previously found is also found in the vicinity of the wall. The instability is visible throughout the entire height of the vessel for measuring lines E and F in the case of the axial velocity component, and measuring line D for the tangential velocity component; however, it is not found in the middle region of the tank. The impeller stream seems to cancel the instability when examined by means of the tangential velocity component.

The significance of the St = 0.0255 instability at the top of the vessel increases when distance to the walls decreases when looking at the axial velocity component. The dimen-

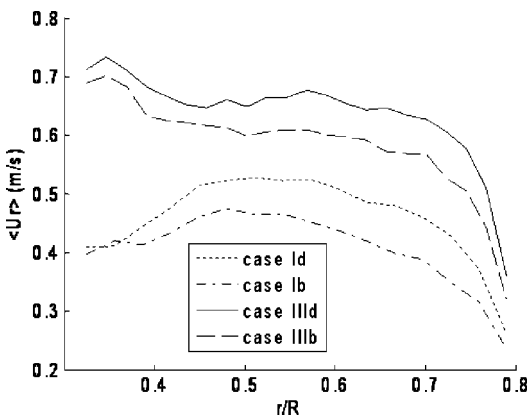

Figure 9. Profiles of the radial velocity on measuring line B in cases Ib, Id, IIId, and IIIb.

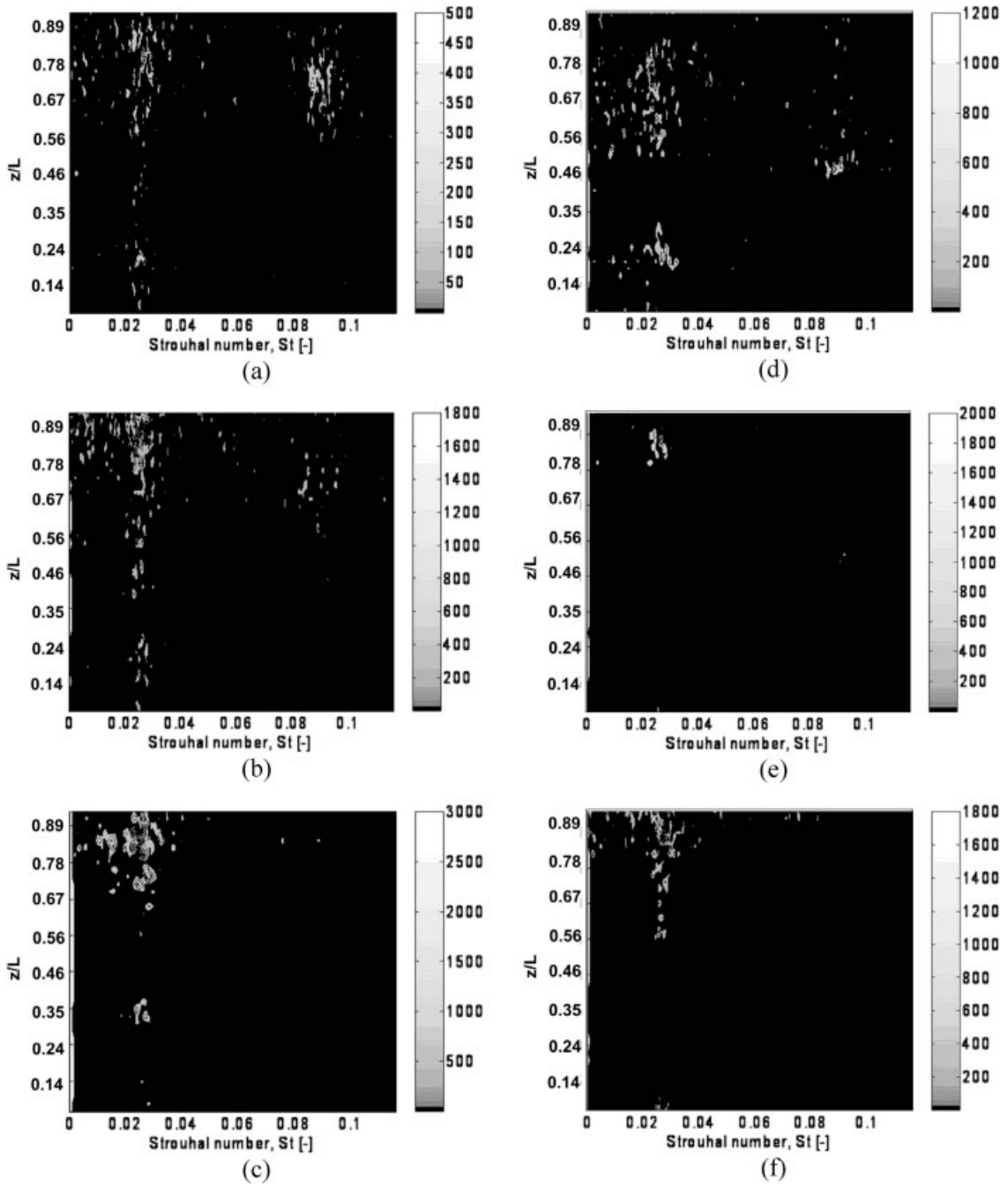

Figure 10. The spatial distribution of macro instabilities near the wall.

Graphs (a), (b), and (c) denote measurement configuration IIc; and graphs (d), (e), and (f) denote IId. The top graphs show measuring line D, the middle graphs show measuring line E, and the bottom graphs show measuring line F.

sionless frequency of 0.0255 corresponds to a time period of 4.55 s in the small vessel using the stirrer speed of 517 rpm. The bandwidth of the St = 0.0255 instability increases when height increases. There is a clear instability at St $\approx$ 0.09 towards the top of the vessel; however, the significance of the instability decreases when distance to the wall decreases. Hartmann et al.[15] have found a characteristic dimensionless frequency of 0.092 in the laminar range. The instability can be attributed to a precessing whirlpool type vortex. Contrary to the St = 0.0255 instability, the St $\approx$ 0.09 instability was not found in the impeller stream. The contour plots for the MI near the wall for the larger vessel were calculated. However, the level of noise was very high.

Conclusions

In this study, periodic instabilities in tanks of various size and geometry were investigated. The macro instabilities were investigated by searching for significant frequencies using the Lomb algorithm for unevenly distributed data. Local in-

stantaneous measurements velocity measurements were obtained using LDA. The instabilities of the flow were visualized using a new type of contour plot, where the energy levels of the entire frequency band of interest were plotted against position. This revealed the spatial distribution of macro instabilities and periodic frequencies related to the passage of blades and the relative importance of these macro instabilities. An important finding of the current study is that the instabilities, in some instances, appear to be very local, making detection difficult.

In the cylindrical configurations, it was found that the harmonics of blade passage differ in both magnitude and spatial distribution. The BPF and the 5th harmonic of the BPF were the most pronounced frequencies both in magnitude and spatial distribution. However, the significance of the only visible BPF harmonic, the 5th BPF, in the square tank configuration diminished rapidly and cannot be distinguished from the background noise at a distance of 1.4 blade widths. This finding is in agreement with Kilander and Rasmuson,[23] where it was found that the periodic contribution of the blade passage only extended four integral lengths from the impeller for a hydro foil impeller.

In the cylindrical tanks, the bandwidth of significant low frequencies broadened from the impeller towards the baffle in both large and small configurations and at both energy inputs. This was not the case in the square configuration, where the distribution in the radial direction was more even.

The time evolution of the velocity in the impeller stream was more erratic in the small cylindrical tank than in the large cylindrical tank. This could be due to the greater inertia of the low frequency fluctuations in the large tank, which had a stabilizing effect on the vortex below the impeller manifested in a constant velocity region just below the impeller jet. This is shown in the velocity profiles in Figure 5. An effect of this can be seen when comparing Figures 3b and 3e, where in the former case more BPF harmonics are clearly visible.

The impeller stream cancelled low frequency fluctuations in a region of $0.5 < r/R < 0.95$ in the small cylindrical tank and of $0.6 < r/R < 0.95$ in the large cylindrical tank. This cancellation cannot be seen close to the tank wall for any of the cylindrical tank configurations. The effect of the impeller stream is visible in the entire frequency band investigated at the height corresponding to the impeller clearance.

A macro instability with the dimensionless frequency Strouhal number St $\approx$ 0.025 was identified in both the impeller stream and the area between the baffles throughout the height of the vessel in the small cylindrical tank with low energy input. Increasing the energy input broadened and scattered the bandwidth of the significant Strouhal number, and the spatial distribution of the St $\approx$ 0.025 was limited to the tank region above the impeller close to the wall. Increasing the size of the vessel, and thus increasing the Reynolds number further, scattered the significant Strouhal numbers; however, the largest amplitudes were still found at St $\approx$ 0.025. This macro instability has been identified previously by Hartmann et al.[15] and was then attributed to a precessing whirlpool type vortex. Further, a macro instability with St $\approx$ 0.09, also identified previously by Hartmann et al.,[15] was detected at the upper part of the tank in the small cylindrical vessel configuration. However the MI was found to be very local, although high in energy, making detection elusive. This could explain why researchers previously have obtained different results. The MI was found for both energy inputs; however, it was much more significant in the low energy case. Two MI were detected for the square configuration. The first, with St $\approx$ 0.06–0.07, was significant both in the upper and lower flow loops; however, it was better defined in the lower flow-loop. The second, with St $\approx$ 0.01 corresponding to a time period of 20.3 s, is clearly visible in the time evolution of the velocity for the impeller stream.

Notation

d = jet diameter, m
D = impeller diameter, m
f_{MI} = macro instability frequency, s^{-1}
H = liquid height, m
L = tank height, m
N = impeller speed, s^{-1}
r = radial position, m
R = tank radius, m
St = dimensionless frequency Strouhal number, $=f_{MI}/N$
U = liquid velocity, m/s
V = tank volume, m^3
W = blade width, m
z = axial position, m

Literature Cited

1. Hasal P, Montes J-L, Boisson, H-C, Fort I. Macro-instabilities of velocity field in stirred vessel: Detection and analysis. *Chem Eng Sci.* 2000;55:391–401.
2. Kresta SM, Wood PE. The mean flow field produced by a 45° pitched blade turbine: changes in the circulations pattern due to off-bottom clearance. *C J Chem Eng.* 1993;71:481–489.
3. Bruha O, Fort I, Smolka P. Flow transition in an axially agitated system. *Proc of the VIII European Conference on Mixing*. Cambridge, UK: IChEME Symposium Series; 1994;136:121.
4. Chapple D, Kresta S. The effect of geometry on the stability of flow patterns in stirred tanks. *Chem Eng Sci.* 1994;21:3651–3660.
5. Bakker A, van der Akker HEA. Single-phase flow in stirred reactors. *Trans Inst Chem Engineers.* 1994;72A:573–582.
6. Montes J-L, Boisson H-C, Fort I, Jahoda M. Velocity field macro-instabilities in an axially agitated mixing vessel. *Chem Eng J.* 1997;67: 139–145.
7. Kresta SM. Turbulence in stirred tanks: anisotropic, approximate and applied. *C J Chem Eng.* 1998;76:563–576.
8. Roussinova V, Kresta SM. Analysis of macro-instabilities (MI) of the flow field in a stirred tank agitated with axial impellers. *Proceedings of 10th European Conference on Mixing*. Delft: Elsevier Science; 2000.
9. Roussinova V, Kresta SM, Weetman R. Low frequency macroinstabilities in a stirred tank: scale-up and prediction based on large eddy simulations. *Chem Eng Sci.* 2003;58:2297–2311.
10. Roussinova V, Kresta SM, Weetman R. Resonant geometries for circulation pattern macroinstabilities in a stirred tank. *AIChE J.* 2004;50:2986 –3005.
11. Galletti C, Brunazzi E, Yianneskis M, Paglianti A. Spectral and wavelet analysis of the flow pattern transition with impeller clearance variations in a stirred vessel. *Chem Eng Sci.* 2003;58:3859–3875.
12. Galletti C, Paglianti A, Lee KC, Yianneskis M. Reynolds number and impeller diameter effects on instabilities in stirred vessels. *AIChE J.* 2004;50:2050–2063.
13. Nikiforaki L, Montante G, Lee KC, Yianneskis M. On the origin, frequency and magnitude of macro-instabilities of the flows stirred in vessels. *Chem Eng Sci.* 2003;58:2937–2949.
14. Yianneskis M, Popiolek Z, Whitelaw JH. An experimental study of the steady and unsteady flow characteristics of stirred vessels. *J Fluid Mech.* 1987;175:537–555.

15. Hartmann H, Derksen JJ, van den Akker HEA. Macroinstability uncovered in a Rushton turbine stirred tank by means of LES. *AIChE J*. 2004;50:2383–2393.
16. Nikiforaki L, Yu J, Baldi S, Genegner B, Lee KC, Durst F, Yianneskis M. On the variation of precessional flow instabilities with operational parameters in stirred vessels. *Chem Eng J*. 2004;102:217–231.
17. Fan J, Wang Y, Rao Q, Fei W. A study on intermittency phenomena in the impeller stream via digital particle image velocimetry (DPIV). *Chem Eng J*. 2004;102:25–33.
18. Nienow AW. Break-up, coalescence and catastrophic phase inversion in turbulent contactors. *Adv Coll Interf Sci*. 2004;108–109:95–103.
19. Lomb NR. Least-squares frequency analysis of unequally spaced data. *Astrophysical J*. 1976;447–462.
20. Kolmogorov AN. The local structure of turbulence in compressible viscous fluid for very large Reynolds numbers. *Doklady Akademii Nauk USSR*. 1941;825–828.
21. Pope SB. *Turbulent Flows*. Cambridge: Cambridge Univ. Press; 2000.
22. Press WH, Flannery BP, Teukolsky SA, Vetterling WT. *Numerical Recipes, the Art of Scientific Computing*. New York: Cambridge Univ. Press; 1992.
23. Kilander J, Rasmuson A. Energy dissipation and macro instabilities in a stirred square tank investigated using a LE PIV approach and LDA measurements. *Chem Eng Sci*. 2005;60:6844–6856.
24. Uhl VW, Gray JB. *Mixing—Theory and Practise*. New York: Academic Press; 1966.
25. Van't Riet K, Bruijn W, Smith JM. Real and pseudo-turbulence in the discharge stream from a Rushton turbine. *Chem Eng Sci*. 1976;31:407–412.
26. Wu H, Patterson GK. Laser-doppler measurements of turbulent-flow parameters in a stirred mixer. *Chem Eng Sci*. 1989;44(10):2207–2221.
27. Pettersson M, Rasmuson Å. Hydrodynamics of suspensions agitated by pitched blade turbine. *AIChE J*. 1998;44:513–527.

Manuscript received Oct. 1, 2005, and revision received Sept. 27, 2006.